

Active-Spin-State-Derived Descriptor for Hydrogen Evolution Reaction Catalysis

Yu Tan,¹ Lei Li,¹ Zi-Xuan Yang,¹ Tao Huang,¹ Qiao-Ling Wang,² Tao Zhang,¹ Jing-Chun Luo,¹ Gui-Fang Huang,^{1*}
Wangyu Hu,³ Wei-Qing Huang^{1*}

¹*Department of Applied Physics, School of Physics and Electronics, Hunan University, Changsha 410082, China*

²*Changsha Environmental Protection College, Changsha 410004, China*

³*School of Materials Science and Engineering, Hunan University, Changsha 410082, China*

Abstract: Spin states are pivotal in modulating the electrocatalytic activity of transition-metal (TM)-based compounds, yet quantitatively evaluating the activity-spin state correlation remains a formidable challenge. Here, we propose an 'activity index (η)' as a descriptor, to assess the activity of the spin states for the hydrogen evolution reaction (HER). η descriptor integrates three key electronic parameters: the proportion (P), broadening range (R) and center (ε_{act}) of active spin state, which collectively account for the electronic structure modulation induced by both the intrinsic active site and its local coordination environment. Using 1T-phase ZrSe₂-anchored TM atoms (TM=Sc to Ni) as prototypes, we reveal that the correlation between Gibbs free energy (ΔG_H) and the η value follows a linear relation, namely, the ΔG_H reduces as the η decreases. Notably, ZrSe₂-Mn exhibits the optimal η value (-0.56), corresponding the best HER activity with a ΔG_H of 0.04 eV—closer to the thermoneutral ideal value (0 eV) than even Pt ($\Delta G_H = -0.09$ eV). This relationship suggests that η is the effective descriptor of active spin state for HER of TM-based catalysts. Our study brings fundamental insights into the HER activity-spin state correlation, offering new strategies for HER catalyst design.

Keywords: hydrogen evolution reaction, transition-metal-based catalyst, spin state, descriptor, linear relationship

*. Corresponding authors: wqhuang@hnu.edu.cn, gfhuang@hnu.edu.cn

Electrochemical water splitting has emerged as a promising approach for efficient, green, and sustainable hydrogen production, yet its scalability is limited by the efficiency and cost of current catalysts.¹⁻⁵ While platinum remains the benchmark for the hydrogen evolution reaction (HER), its scarcity drives urgent efforts to develop earth-abundant alternatives.⁶⁻¹¹ Typically, the rational design of HER catalysts primarily focuses on tuning electronic properties, including valence states and *d*-band center positions.¹²⁻¹⁸

Recent experimental and theoretical investigations demonstrate the critical role of spin states in transition metal (TM)-based catalysts, offering an underexplored avenue to tailor catalytic activity beyond traditional electronic structure modulation.¹⁹⁻²³ In TM-based single-atom catalysts (SACs), high-spin (HS) and low-spin (LS) configurations exhibit distinct interactions with reaction intermediates, enabling spin-dependent reactivity. For instance, for oxygen evolution reaction (OER) process, Co³⁺ in HS state facilitates stronger *d-p* orbital overlap with oxygen-containing species, lower the energy barrier for O-O bond formation and promote the adsorption of OOH intermediates, a rate-limiting step in OER.^{24,25} Similarly, Fe-based HS catalysts exhibit enhanced OER activity due to spin-selective charge transfer, where unpaired electrons mediate efficient hole injection into adsorbed OH⁻ species.²⁶ For HER, LS Ni²⁺ in NiSe₂ exhibits excellent activity due to reduced Pauli repulsion between filled *d*-orbitals and H 1*s* orbital, weakening H^{*} binding and enabling rapid desorption of H₂.²⁷

More recently, our work has demonstrated that spin states in TM-based catalysts can be categorized into *active* and *inert* spin states.²⁰ Only the active spin state, characterized by unpaired electrons in symmetry-adapted orbitals (such as, out-of-plane *d*_{z²} orbital), can significantly modulate hydrogen adsorption strength through symmetry matching with the H-1*s* orbital. In contrast, the inert spin states with in-plane unpaired electron (such as, *d*_{x²-y²} orbital), exhibit negligible contributions due to symmetry mismatch.²⁰ However, this simplified binary classification overlooks the complexity of spin-polarized systems. For example, Mn or Fe based catalyst on sulfur-rich supports (such as MoS₂) may exhibit distinct spin-dependent behaviors due to stronger metal-support charge transfer.²⁸⁻³⁰ Furthermore, while the qualitative distinction between active and inert states is established, the quantitative correlation between the HER activity and active spin states remains unresolved. Addressing these gaps requires establishing correlations between adsorption

energetics and spin states, coupled with multi-component interactions within catalyst-support systems, thereby advancing spin state engineering for enhanced HER performance.

Here, we address these challenges by developing a quantitative activity-spin state descriptor for HER, validated across a range of earth-abundant SACs. Specifically, we propose an 'activity index (η)' as a descriptor, which account for the electronic structure modulation induced by both the intrinsic active site and its local coordination environment, to assess the activity of the spin states for HER. Taking 1T-phase ZrSe₂ anchoring TM atoms (TM=Sc to Ni) as models, a linear dependence is found between Gibbs free energy (ΔG_{H}) and the η value, with ΔG_{H} declining as η decreases. This correlation indicates that the η can serve as the effective descriptor for the active spin state in HER on TM-based catalysts. Our work provides fundamental insights into the activity-spin state relationship, offering new avenues for HER catalyst design.

Firstly, we investigate the geometric structure and electronic properties of the 1T-phase ZrSe₂. As shown in Fig. 1 (a), the Zr atomic layer is sandwiched between two Se atomic layers, which are staggered relative to each another, forming an octahedral coordination structure. The optimized lattice constants are $a = b = 3.793 \text{ \AA}$, and the Zr-Se bond length is $d = 2.707 \text{ \AA}$, which are in agreement with previous results.³¹ Here, we employ an anchoring strategy to obtain the SACs. As illustrated in Fig. 1 (b), we select the position directly above the Zr atom as the anchoring site for TM atoms, including Sc, Ti, V, Cr, Mn, Fe, Co and Ni from the fourth period. Table S1 lists the lattice constant of the eight ZrSe₂-TM systems, which remain largely unchanged. All binding energies (Table S1) are negative, indicating that these systems are energetically stable.

The electronic properties of ZrSe₂-TM systems are fundamentally altered by the introduction of the anchored TM atoms. As illustrated in Fig. 1 (c), the calculated band structure and density of states (DOS) reveal that pristine ZrSe₂ is a non-magnetic semiconductor with a band gap of 0.497eV. However, the anchored TM atoms induce a semiconductor-to-metal transition in ZrSe₂-TM systems — except for ZrSe₂-Ni — as evidenced by the total DOS of these systems in Fig. S1. Furthermore, ZrSe₂-Ni remains non-magnetic, while the other systems exhibit magnetic behavior, with their total magnetic moments listed in Table S1.

The SACs with tunable electronic properties upon the same anchoring strategy exhibit interesting catalytic behavior. To evaluate the HER activity of ZrSe₂-TM systems, we calculate the

Gibbs free energy (ΔG_H) of hydrogen adsorption by positioning H atoms at the top site of the anchored TM atoms. The optimized configurations are shown in Fig. S2. As illustrated in Fig. 2 (a), the ΔG_H exhibits a two-segment increasing trend as the anchored TM atom varies from Sc to Ni. Specifically, when the TM atom transitions from Sc to Cr, the ΔG_H increases from -0.10 to 2.68 eV. In the second segment, when the TM atom varies from Mn to Ni, the ΔG_H increases from -0.04 to 1.06 eV. Notably, ZrSe₂-Mn exhibits the best HER activity with a ΔG_H of 0.04 eV, which is closer to the thermoneutral ideal value (0 eV) than even Pt ($\Delta G_H = -0.09$ eV).

The d -band center (ε_d) is commonly used to explain the activity of metal and metal-based catalysts, where a higher position of ε_d typically correlates with stronger adsorption strength.^{32,33} For the ZrSe₂-TM systems studied here, however, the ε_d fails to fully account for the observed ΔG_H variation. As illustrated in Fig. 2 (b), the ε_d exhibits a monotonic decrease (except for the ZrSe₂-Ni semiconductor), which contrasts sharply with the two-segment increasing trend of ΔG_H . Actually, the decrease of ε_d is due to electron count changes: from ZrSe₂-Sc to ZrSe₂-Ni, the valence electron count of the anchored TM atoms increases while the transfer electron (Table S1) continuously decreases. Consequently, the increased electron occupation (Fig. 2 (c)) leads to more d -orbitals being filled below the Fermi level (E_F), thus lowering the ε_d . As a special case, ZrSe₂-Ni maintains a relatively high ε_d due to upward d -orbital shifting induced by the semiconductor bandgap. The observed decoupling between the ε_d and HER activity indicates that the underlying mechanism beyond conventional d -band theory governs the catalytic performance in these systems, requiring further investigation.

Interestingly, a surprising correlation between the magnetic moments of anchored TM atoms and their corresponding ΔG_H is observed in the ZrSe₂-TM systems. As shown in Fig. 2 (d), the magnetic moments also exhibit an evident two-segment trend: they increase from Sc to Cr, then decrease from Mn to Ni. This trend strongly suggests that the hydrogen adsorption strength is primarily governed by spin-polarized electronic states, rather than the collective d -band effects. Crucially, the localized states near E_F , predominantly originating from the anchored TM atoms (Fig. S1), mediate the observed magnetism and likely drive this spin-dependent adsorption mechanism.

In fact, the ε_d parameter fundamentally accounts for all d -orbitals, thus all possible adsorbate- d -orbital interactions, but only symmetry-allowed couplings contribute under the selection rules of

chemical bonding. At the atop adsorption site of TM atom, the d_{z^2} orbital exhibits symmetry compatibility with the H-1s orbital, forming a σ bond, as shown in Fig. 2 (e). Orbital-projected density of states (PDOS) analysis (Fig. 3) reveals that the localized states (dashed box region) predominantly originate from the d_{z^2} orbital, identifying these as real active states. This is further corroborated by pronounced orbital overlap between the TM- d_{z^2} and H-1s orbitals near E_F , as evidenced by wavefunction projection analysis (Figs. 4 and S3). We therefore define these spin-polarized d_{z^2} orbitals as active spin states, whose strong hybridization with H-1s governs hydrogen adsorption strength. Conversely, in non-spin-polarized ZrSe₂-Ni system, the d_{z^2} orbital is inert state that show negligible participation in H adsorption.

As illustrated in Fig. 3, the active spin states in ZrSe₂-TM systems evolve through three distinct configurations governed by d -orbital filling: i) In ZrSe₂-Sc system, the single d electron occupies the spin-up d -orbital, forming a high-spin state consistent with Hund's rule; ii) For ZrSe₂-Ti to ZrSe₂-V, d electron partial filling of both spin channels creates intermediate-spin configurations, with ZrSe₂-Cr system recovering a high-spin state when spin-up orbitals become fully occupied by d electrons; iii) Beyond half-filling (ZrSe₂-Mn to ZrSe₂-Ni), progressive spin-down occupation reduces polarization, culminating in ZrSe₂-Ni's non-magnetic state with balanced spin-up/down populations. This evolution of spin states reflects the competition between exchange splitting and Coulomb repulsion --- while high-spin states dominate when exchange splitting is large, spin degeneracy emerges upon complete d -shell filling. Crucially, the d_{z^2} orbital's spin polarization directly modulates its hybridization strength with H-1s (Figs. 4 and S3), confirming active spin states as the primary determinant of hydrogen adsorption energetics.

Based on the above analysis, as illustrated in Figure 5 (a) (right panel), we propose two idealized types of active spin states. i) Unpaired electron occupation of the d_{z^2} orbital: When only one electron occupies the d_{z^2} orbital, it preferentially occupies the spin-up state (such as ZrSe₂-Sc). This unpaired electron actively participates in the reaction, consistent with previous studies.²⁰ ii) Partial-fully occupied d_{z^2} orbital: When the spin-up state of the d_{z^2} orbital is fully occupied, additional electrons populate the spin-down orbital. Under spin-polarized conditions, the spin-down electron serves as the active spin state, while the spin-up electrons are non-bonding (such as ZrSe₂-Mn). Interestingly, for the ZrSe₂-TM system, we find that with increased number of valence

electrons, the first type of active spin state can evolve into a low-spin state with half spin-up and half spin-down occupancy (such as ZrSe₂-Ti), representing a special case of active spin state. In contrast, the second type of active spin state becomes inert after depolarization (such as ZrSe₂-Ni). This is verified by the statistical analysis of electron populations in active states (Fig. S4): except for the inert state of ZrSe₂-Ni, which has two electrons, all other active spin states exhibit approximately one electron. Regardless of the type of active spin state, only one electron in the d_{z^2} orbital forms a bond with the H 1s orbital, resulting in a fully occupied bonding state and an unoccupied antibonding state. According to molecular orbital theory, this leads to a stronger bonding interaction between the anchored TM atom and hydrogen, thereby enhancing hydrogen adsorption.

In contrast, the d_{z^2} orbital of ZrSe₂-Ni, representing an inert state, exhibits spin degeneracy and is relatively far from E_F (Fig. 3). The number of d_{z^2} electrons in the active spin state or inert state is displayed in Fig. S4, showing about 2 for ZrSe₂-Ni but 1 for others. This means that the d_{z^2} orbital is fully occupied and its depolarization originates from the second type. As illustrated in Fig. 5 (a) (left panel), the interaction between two electrons in d_{z^2} orbital with the H-1s orbital results in two electrons occupying the bonding orbital and one electron occupies the antibonding orbital. This partial occupancy of antibonding state introduces energetic destabilization of the Ni-H bond, elevates total electronic energy of the system and weakens H adsorption strength. As illustrated in Fig. 4 (d), for ZrSe₂-Ni, the interaction between the inert state and H-1s orbital is negligible. The result of -COHP reveals antibonding Ni-H interactions, leading to weak adsorption of the H atom.

Two types of active spin state require refinement in real systems due to substrate-mediated orbital modulation and coordination field effects. Based on the maximum overlap principle of molecular orbital theory, the modified d_{z^2} orbital wavefunction of active spin states (Fig. S5) due to d -orbital hybridization and substrate interactions, reduces spatial overlap with H-1s orbitals, thereby reducing the hydrogen adsorption strength. We quantify this effect through the *active spin state proportion* (P), defined as the weight of active spin states within localized states (Fig. 3). As shown in Fig. 5 (b), P decreases across two transition sequences: Sc→Cr (from 0.97 to 0.28) and Mn→Co (from 0.97 to 0.31), directly correlating with weakened interaction between active spin

states and H-1s orbital, align with the observed ΔG_H trend. Furthermore, we introduce the **state broadening range** (R), defined as the energy span of active spin states, to assess the interactions between d_{z^2} and other orbitals. [Figure 5 \(c\)](#) demonstrates the increased R values along Sc→Cr (from 0.40 to 1.80 eV) and Fe→Ni (from 0.27 to 1.50 eV) sequences, reflecting enhanced delocalization of active spin states. This dual mechanism—reduced hybridization and increased delocalization—synergistically weakens overlap between active spin states and the H-1s orbital, ultimately degrading hydrogen adsorption capability.

Frontier orbital theory further dictates that only the states near the E_F contribute to catalytic activity.³⁴ Consequently, the d_{z^2} orbitals far from the E_F possess negligible influence on the activity, and are thus excluded from the active spin states. This indicates that the distance between the active spin states and E_F plays a critical role in determining the catalytic activity. Therefore, we define the **active spin state center**, ε_{act} , where ε_{act} is the integration center of the active spin state. As illustrated in [Fig. 5 \(d\)](#), ε_{act} shifts downward as the anchored atom varies from Ti to Cr (-0.58 to -1.43 eV) and from Mn to Ni (-0.65 to -1.94 eV), moving the active spin states away from the E_F , and aligning with the increase in ΔG_H . This trend aligns with the frontier orbital theory, where states closer to E_F exhibit higher reactivity.

However, none of the three individual descriptors can universally account for the catalytic behavior of the studied systems, as their catalytic activity arises from their synergistic interaction among multiple factors. To address this, we propose a unified descriptor — the logarithmic activity index (η) — defined as:

$$\eta = \log (|\varepsilon_{act}| \cdot \frac{R}{P})$$

where ε_{act} represents the energy difference between E_F and integration center of the active spin state, R denotes the broadening range of active spin states, and P is the proportion of active spin state in localized state.

The activity index η demonstrates robust predictive capability for the HER performance across all ZrSe₂-TM systems. As illustrated in [Fig. 5 \(e\)](#), when the anchored atom varies from Sc to V, the linear correlation between ΔG_H and η is described by: $\Delta G_H = 0.3712 + 1.0415\eta$. Similarly, for the anchored TM atoms ranging from Mn to Ni, the relationship is given by: $\Delta G_H = 0.5507 + 1.0435\eta$.

The corresponding coefficients of determination (R^2) are 0.9920 and 0.9998, respectively, underscoring the strong linear correlation between ΔG_H and η . The nearly identical slopes of the two fits further validate the robustness and transferability of η in quantifying the influence of active spin states. According to the Sabatier principle, optimal catalytic performance is achieved when the binding strength between the catalyst and reaction intermediates is neither too strong nor too weak.^{35–37} As shown in Fig. 5 (e), a smaller η value corresponds to a ΔG_H closer to thermoneutrality, indicating enhanced HER activity. Among all the TM-based SACs, ZrSe₂-Mn has the optimal η (-0.56), which exhibits the best HER activity with a ΔG_H of 0.04 eV. This makes η an effective and convenient screening parameter for identifying catalysts with superior intrinsic activity. Thus, η serves as a reliable and generalizable descriptor for capturing variations in hydrogen adsorption energetics. It not only provides fundamental insights into HER mechanisms but also enables the rational design of spin-state-engineered electrocatalysts.

In summary, we have investigated HER catalysis by different spin states of TM SACs supported on ZrSe₂ using DFT calculations. Two types of active spin states are pinpointed. Considering the electronic structure modulation induced by both the intrinsic active site and its local coordination environment, we propose a descriptor— activity index (η)— to assess the activity of the spin states for HER. We demonstrate a nearly linear relationship between the ΔG_H and the η value, which fits a relation of $\Delta G_H = 0.3712 + 1.0415\eta$ ($\Delta G_H = 0.5507 + 1.0435\eta$) with the determination coefficient R^2 as 0.9920 (0.9998). This thus suggests that activity index η is a promising HER catalytic descriptor for TM-based catalysts. Our findings provide important insight into the relationship between HER activity and spin, offering new designing strategies for TM-based catalysts.

SUPPLEMENTARY MATERIALS

See the [supplementary material](#) for the computational methods and additional results.

ACKNOWLEDGEMENTS

This work was supported by the National Natural Science Foundation of China (Grants No.

52172088) and Basic and Applied Basic Research Foundation of Guangdong Province (No. 2024A1515010421).

DATA AVAILABILITY

The data that support the findings of this study are available within the article and its [supplementary material](#).

REFERENCES

- ¹ B.H.R. Suryanto, Y. Wang, R.K. Hocking, W. Adamson, and C. Zhao, “Overall electrochemical splitting of water at the heterogeneous interface of nickel and iron oxide,” *Nat. Commun.* **10**(1), 5599 (2019).
- ² H. Dotan, A. Landman, S.W. Sheehan, K.D. Malviya, G.E. Shter, D.A. Grave, Z. Arzi, N. Yehudai, M. Halabi, N. Gal, N. Hadari, C. Cohen, A. Rothschild, and G.S. Grader, “Decoupled hydrogen and oxygen evolution by a two-step electrochemical–chemical cycle for efficient overall water splitting,” *Nat. Energy.* **4**(9), 786–795 (2019).
- ³ J. Nie, J. Shi, L. Li, M. Xie, Z. Ouyang, M. Xian, G. Huang, H. Wan, W. Hu, and W. Huang, “Dense Crystalline-Amorphous Nano-Interfaces Derived from Local Reconstruction for Alkaline Hydrogen Evolution,” *Advanced Energy Materials.* **15**(11), 2404246 (2025).
- ⁴ I. Roger, M.A. Shipman, and M.D. Symes, “Earth-abundant catalysts for electrochemical and photoelectrochemical water splitting,” *Nat. Rev. Chem.* **1**(1), 0003 (2017).
- ⁵ Q. Qian, Y. Zhu, N. Ahmad, Y. Feng, H. Zhang, M. Cheng, H. Liu, C. Xiao, G. Zhang, and Y. Xie, “Recent Advancements in Electrochemical Hydrogen Production via Hybrid Water Splitting,” *Advanced Materials.* **36**(4), 2306108 (2024).
- ⁶ R. Kronberg, and K. Laasonen, “Reconciling the Experimental and Computational Hydrogen Evolution Activities of Pt(111) through DFT-Based Constrained MD Simulations,” *ACS Catal.* **11**(13), 8062–8078 (2021).
- ⁷ Y. Li, X. Tan, R.K. Hocking, X. Bo, H. Ren, B. Johannessen, S.C. Smith, and C. Zhao, “Implanting Ni-O-VO_x sites into Cu-doped Ni for low-overpotential alkaline hydrogen evolution,” *Nat. Commun.* **11**(1), 2720 (2020).
- ⁸ X. Ding, D. Liu, P. Zhao, X. Chen, H. Wang, F.E. Oropeza, G. Gorni, M. Barawi, M. García-Tecedor, V.A. De La Peña O’Shea, J.P. Hofmann, J. Li, J. Kim, S. Cho, R. Wu, and K.H.L. Zhang, “Dynamic restructuring of nickel sulfides for electrocatalytic hydrogen evolution reaction,” *Nat. Commun.* **15**(1), 5336 (2024).
- ⁹ S. Sultan, J.N. Tiwari, A.N. Singh, S. Zhumagali, M. Ha, C.W. Myung, P. Thangavel, and K.S. Kim, “Single Atoms and Clusters Based Nanomaterials for Hydrogen Evolution, Oxygen Evolution Reactions, and Full Water Splitting,” *Advanced Energy Materials.* **9**(22), 1900624 (2019).
- ¹⁰ X. Huang, X. Xu, X. Luan, and D. Cheng, “CoP nanowires coupled with CoMoP nanosheets as a highly efficient cooperative catalyst for hydrogen evolution reaction,” *Nano Energy.* **68**, 104332 (2020).
- ¹¹ Y. Zheng, Y. Jiao, L.H. Li, T. Xing, Y. Chen, M. Jaroniec, and S.Z. Qiao, “Toward Design of Synergistically Active Carbon-Based Catalysts for Electrocatalytic Hydrogen Evolution,” *ACS Nano* **8**(5), 5290–5296 (2014).
- ¹² Y. Shi, Z.-R. Ma, Y.-Y. Xiao, Y.-C. Yin, W.-M. Huang, Z.-C. Huang, Y.-Z. Zheng, F.-Y. Mu, R. Huang, G.-Y. Shi, Y.-Y. Sun, X.-H. Xia, and W. Chen, “Electronic metal–support interaction modulates single-atom platinum catalysis for hydrogen evolution reaction,” *Nat. Commun.* **12**(1), 3021 (2021).
- ¹³ L. Li, T. Huang, K. Liang, Y. Si, J.-C. Lian, W.-Q. Huang, W. Hu, and G.-F. Huang, “Symmetry-Breaking-Induced Multifunctionalities of Two-Dimensional Chromium-Based Materials for Nanoelectronics and Clean Energy Conversion,” *Phys. Rev. Applied.* **18**(1), 014013 (2022).
- ¹⁴ S. Jiao, X. Fu, and H. Huang, “Descriptors for the Evaluation of Electrocatalytic Reactions: d-Band Theory and Beyond,” *Adv. Funct. Mater.* **32**(4), 2107651 (2022).

- ¹⁵ B. Cao, M. Hu, Y. Cheng, P. Jing, B. Liu, B. Zhou, X. Wang, R. Gao, X. Sun, Y. Du, and J. Zhang, “Tailoring the d-band center of N-doped carbon nanotube arrays with Co₄N nanoparticles and single-atom Co for a superior hydrogen evolution reaction,” *NPG. Asia. Mater.* **13**(1), 1 (2021).
- ¹⁶ Q. Hu, K. Gao, X. Wang, H. Zheng, J. Cao, L. Mi, Q. Huo, H. Yang, J. Liu, and C. He, “Subnanometric Ru clusters with upshifted D band center improve performance for alkaline hydrogen evolution reaction,” *Nat. Commun.* **13**(1), 3958 (2022).
- ¹⁷ X. Wang, X. Xu, Y. Nie, R. Wang, and J. Zou, “Electronic-State Modulation of Metallic Co-Assisted Co₇ Fe₃ Alloy Heterostructure for Highly Efficient and Stable Overall Water Splitting,” *Advanced Science.* **10**(22), 2301961 (2023).
- ¹⁸ Y. Chen, Y. Liu, W. Zhai, H. Liu, T. Sakhivel, S. Guo, and Z. Dai, “Metastabilizing the Ruthenium Clusters by Interfacial Oxygen Vacancies for Boosted Water Splitting Electrocatalysis,” *Advanced Energy Materials.* **14**(21), 2400059 (2024).
- ¹⁹ Y. Huang, S. Li, Z. Zhang, and P. Cui, “Synergistic role of p – d hybridization and magnetism in enhanced water splitting on ferromagnetic 1 T transition metal dichalcogenides,” *Phys. Rev. B* **109**(19), 195414 (2024).
- ²⁰ T. Zhang, L. Li, T. Huang, H. Wan, W.-Y. Chen, Z.-X. Yang, G.-F. Huang, W. Hu, and W.-Q. Huang, “Correlation between spin state and activity for hydrogen evolution of PtN₂ monolayer,” *Appl. Phys. Lett.* **124**(6), 063903 (2024).
- ²¹ N. Mulakaluri, R. Pentcheva, M. Wieland, W. Moritz, and M. Scheffler, “Partial Dissociation of Water on Fe₃O₄(001): Adsorbate Induced Charge and Orbital Order,” *Phys. Rev. Lett.* **103**(17), 176102 (2009).
- ²² F.A. Garcés-Pineda, M. Blasco-Ahicart, D. Nieto-Castro, N. López, and J.R. Galán-Mascarós, “Direct magnetic enhancement of electrocatalytic water oxidation in alkaline media,” *Nat. Energy.* **4**(6), 519–525 (2019).
- ²³ Z. Chen, X. Li, H. Ma, Y. Zhang, J. Peng, T. Ma, Z. Cheng, J. Gracia, Y. Sun, and Z.J. Xu, “Spin-dependent electrocatalysis,” *National Science Review.* **11**(9), nwae314 (2024).
- ²⁴ B. Ge, P. Jiang, B. Chen, and C. Huang, “Controlling Co 3d/O 2p Orbital Hybridization in LaCoO₃ by Modulating the Co–O–Co Bond Angle for Enhanced Oxygen Evolution Reaction Catalysis,” *ACS Catal.* **15**(1), 477–486 (2025).
- ²⁵ X. Zhang, H. Zhong, Q. Zhang, Q. Zhang, C. Wu, J. Yu, Y. Ma, H. An, H. Wang, Y. Zou, C. Diao, J. Chen, Z.G. Yu, S. Xi, X. Wang, and J. Xue, “High-spin Co³⁺ in cobalt oxyhydroxide for efficient water oxidation,” *Nat. Commun.* **15**(1), 1383 (2024).
- ²⁶ L.-L. Hao, J.-Y. Hu, J. Li, Y.-J. Gao, Y.-S. Meng, and T. Liu, “Manipulating the Intrinsic Magnetism of Spinel Catalyst toward Magnetic Field-Enhanced OER,” *ACS Catal.* **15**(7), 5640–5650 (2025).
- ²⁷ R.D. Smyth, J.N. Blandy, Z. Yu, S. Liu, C.V. Topping, S.J. Cassidy, C.F. Smura, D.N. Woodruff, P. Manuel, C.L. Bull, N.P. Funnell, C.J. Ridley, J.E. McGrady, and S.J. Clarke, “High- versus Low-Spin Ni²⁺ in Elongated Octahedral Environments: Sr₂ NiO₂ Cu₂ Se₂, Sr₂ NiO₂ Cu₂ S₂, and Sr₂ NiO₂ Cu₂ (Se_{1-x} S_x)₂,” *Chem. Mater.* **34**(21), 9503–9516 (2022).
- ²⁸ Y. Zhang, K. Shinokita, K. Watanabe, T. Taniguchi, M. Goto, D. Kan, Y. Shimakawa, Y. Moritomo, T. Nishihara, Y. Miyauchi, and K. Matsuda, “Controllable Magnetic Proximity Effect and Charge Transfer in 2D Semiconductor and Double-Layered Perovskite Manganese Oxide van der Waals Heterostructure,” *Advanced Materials.* **32**(50), 2003501 (2020).
- ²⁹ V. Ortiz Jimenez, Y.T.H. Pham, D. Zhou, M. Liu, F.A. Nugera, V. Kalappattil, T. Eggers, K. Hoang,

D.L. Duong, M. Terrones, H. Rodriguez Gutiérrez, and M. Phan, “Transition Metal Dichalcogenides: Making Atomic-Level Magnetism Tunable with Light at Room Temperature,” *Advanced Science*. **11**(7), 2304792 (2024).

³⁰ H. Tan, C. Wang, W. Hu, H. Duan, P. Guo, N. Li, G. Li, L. Cai, Z. Sun, F. Hu, and W. Yan, “Reversible Tuning of the Ferromagnetic Behavior in Mn-Doped MoS₂ Nanosheets via Interface Charge Transfer,” *ACS Appl. Mater. Interfaces*. **10**(37), 31648–31654 (2018).

³¹ T.V. Vu, H.D. Tong, D.P. Tran, N.T.T. Binh, C.V. Nguyen, H.V. Phuc, H.M. Do, and N.N. Hieu, “Electronic and optical properties of Janus ZrSSe by density functional theory,” *RSC Adv*. **9**(70), 41058–41065 (2019).

³² B. Hammer, and J.K. Nørskov, “Electronic factors determining the reactivity of metal surfaces,” *Surface Science*. **343**(3), 211–220 (1995).

³³ H. Xin, A. Vojvodic, J. Voss, J.K. Nørskov, and F. Abild-Pedersen, “Effects of d -band shape on the surface reactivity of transition-metal alloys,” *Phys. Rev. B*. **89**(11), 115114 (2014).

³⁴ K. Liu, J. Fu, Y. Lin, T. Luo, G. Ni, H. Li, Z. Lin, and M. Liu, “Insights into the activity of single-atom Fe-N-C catalysts for oxygen reduction reaction,” *Nat. Commun*. **13**(1), 2075 (2022).

³⁵ A.B. Laursen, A.S. Varela, F. Dionigi, H. Fanchiu, C. Miller, O.L. Trinhammer, J. Rossmeisl, and S. Dahl, “Electrochemical Hydrogen Evolution: Sabatier’s Principle and the Volcano Plot,” *J. Chem. Educ*. **89**(12), 1595–1599 (2012).

³⁶ H. Ooka, J. Huang, and K.S. Exner, “The Sabatier Principle in Electrocatalysis: Basics, Limitations, and Extensions,” *Front. Energy Res*. **9**, 654460 (2021).

³⁷ J. Nie, J. Shi, L. Li, M.-Y. Xie, Z.-Y. Ouyang, M.-H. Xian, G.-F. Huang, H. Wan, W. Hu, and W.-Q. Huang, “Spatial/electronic symmetry breaking of metal-support catalysts for efficient water dissociation and alkaline hydrogen spillover,” *Nano Energy*. **138**, 110873 (2025).

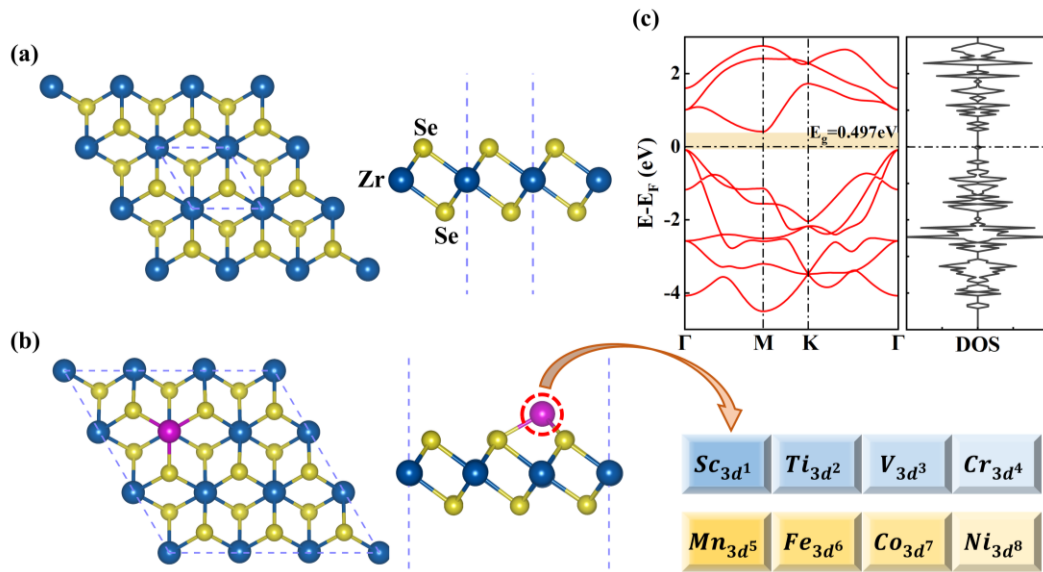


FIG. 1. The structure, electronic properties and anchoring atoms of 1T-ZrSe₂. (a) The top and side views and (c) electronic band structure and density of state of 1T-ZrSe₂. The Fermi level is set to zero. (b) The top and side views of 1T-ZrSe₂-TM with primitive unit cell shown by the dashed line. On the right are electron configurations of the eight fourth period metal elements anchored on ZrSe₂.

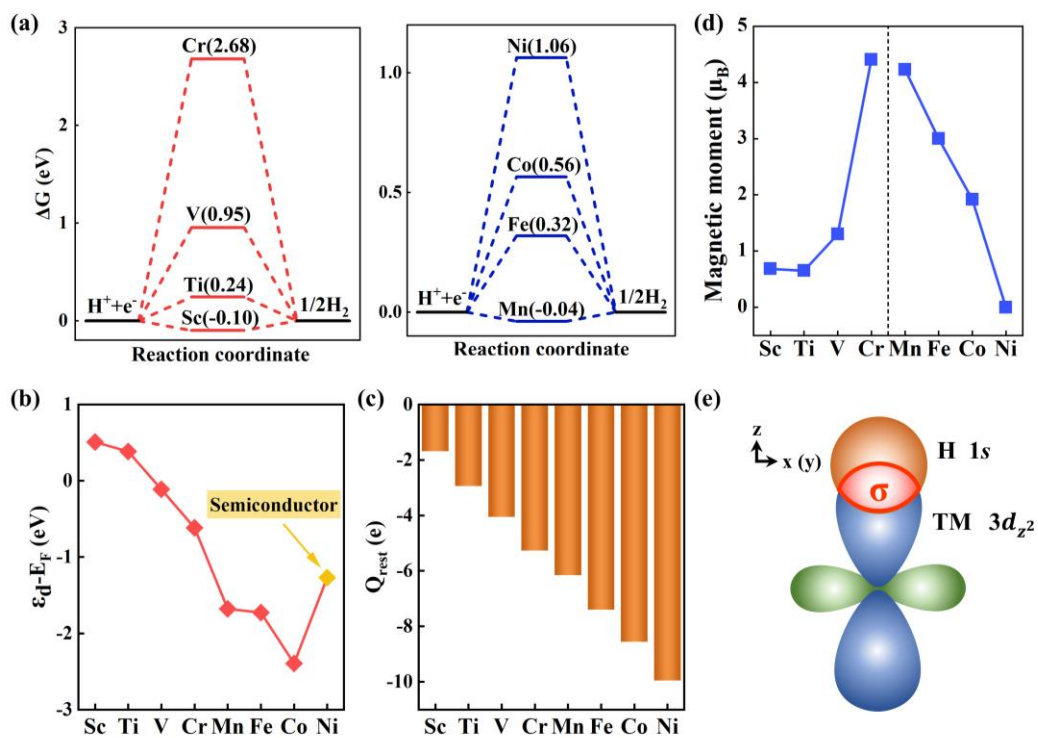


FIG. 2. Calculated Gibbs free energy diagram for HER on TM site of (a1) ZrSe₂-TM (TM=Sc, Ti, V, Cr) and (a2) ZrSe₂-TM (TM=Mn, Fe, Co, Ni). The (b) d-band center, (c) residual electron and (d) magnetic moment of TM atom of ZrSe₂-TM. (e) Diagram of TM-H orbit interaction.

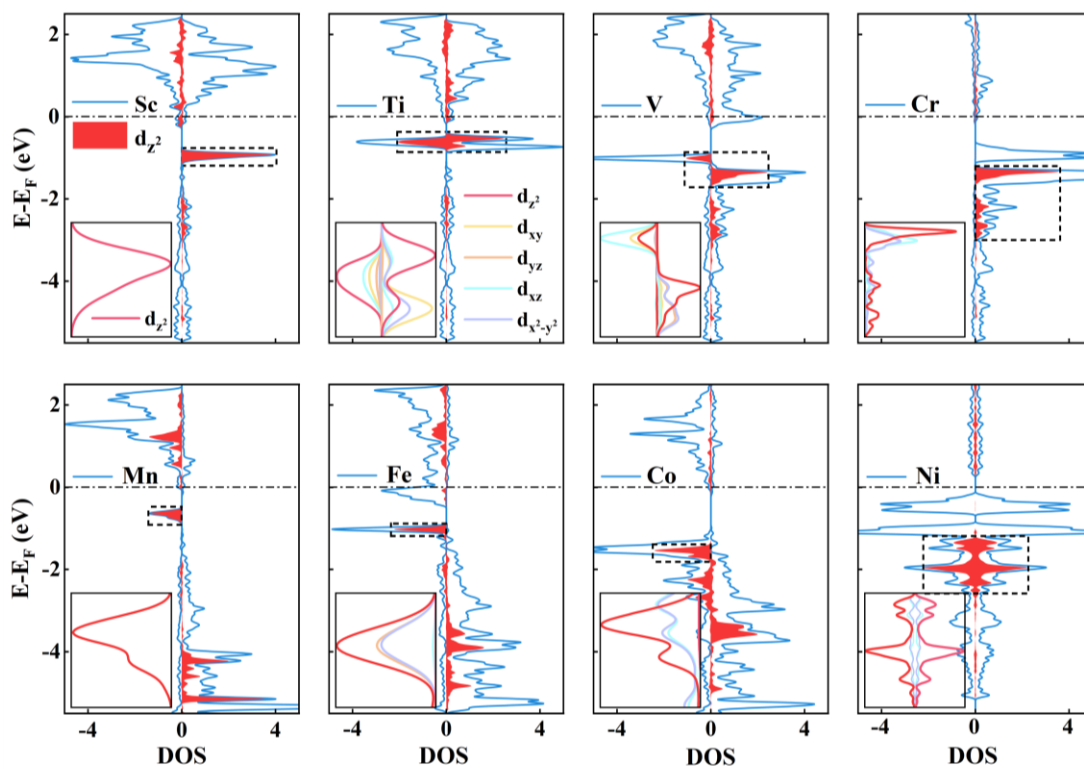


FIG. 3. The PDOS of $\text{ZrSe}_2\text{-TM}$ (TM = Sc, Ti, V, Cr, Mn, Fe, Co, Ni) and local magnification of the active spin states. The local magnification in the lower left corner is the local enlargement in the d orbital of five directions of the state boxed by dashed line. The Fermi levels are set to zero.

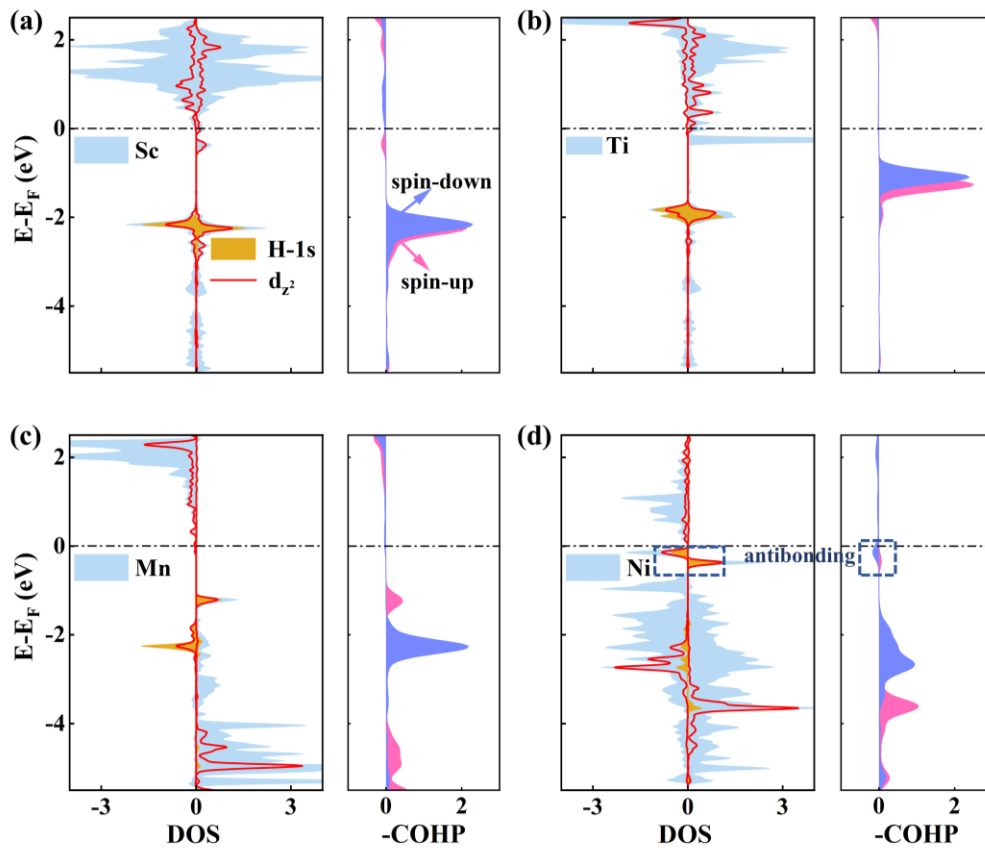


FIG. 4. The PDOS and -COHP of $\text{ZrSe}_2\text{-TM-H}^*$ (TM = Sc, Ti, Mn, Ni). The Fermi levels are set to zero.

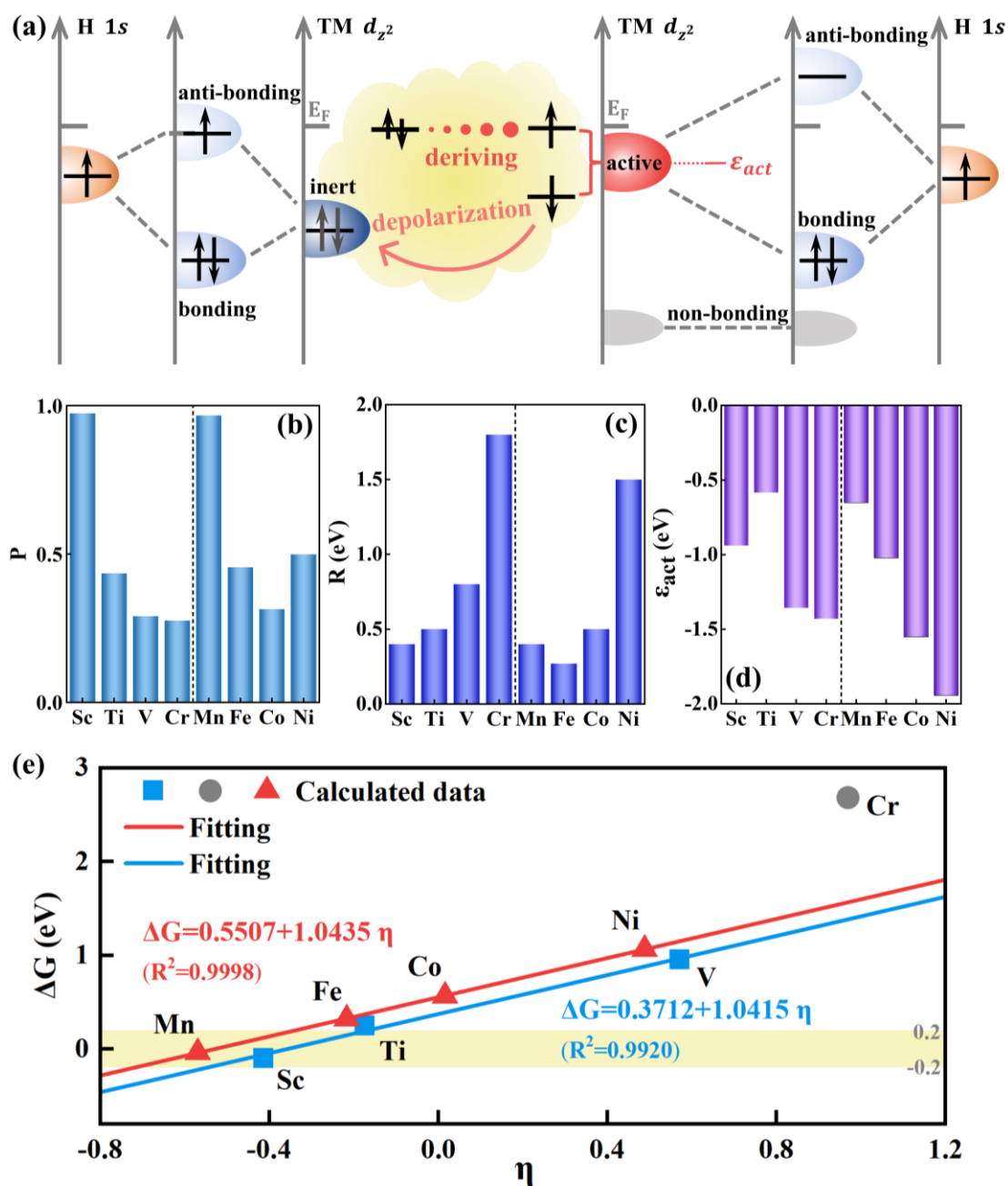


FIG. 5. The HER mechanism of active spin states. (a) Diagram of the interaction between the active spin state (inert state) and H-1s, two idealized types of the active spin states and relationship between the active spin state and inert state. The (b) *proportion* P, (c) *broadening range* R and (d) *center* ϵ_{act} of active spin states. (e) Linear relation between the logarithmic activity index η and Gibbs free energy ΔG .